FEBS Letters 581 (2007) 5469–5474

Histological mapping of biochemical changes in solid tumors by FT-IR spectral imaging

Cyril Petibois[a,b,*], Benjamin Drogat[c,d], Andreas Bikfalvi[c,d], Gérard Déléris[a,b], Michel Moenner[c,d]

[a] University of Bordeaux 2, CNRS, UMR 5084, 146 Rue Léo Saignat, F33076, Bordeaux, France
[b] CNRS, UMR 5084, CNAB, Bio-Organic Chemistry Group, Bordeaux F-33076, France
[c] Inserm, E0113, Talence F-33400, France
[d] University of Bordeaux, Univ Bordeaux 1, Talence F-33400, France

Received 8 June 2007; revised 15 October 2007; accepted 25 October 2007

Available online 5 November 2007

Edited by Richard Marais

Abstract **Fourier-transform infrared (FT-IR) spectral imaging was used for analyzing biochemical changes in tumor cells. Metabolic parameters of human lung A549/8 adenocarcinoma and U87 glioma cells were compared under stress conditions in culture along with tumor progression after cell implantation onto the chick embryo chorio-allantoic membrane. In cell culture, glucose consumption and lactic acid release were higher in U87 cells. A549/8 cells were less sensitive to oxidative stress as observed through changes in fatty acyl chains. In vivo biochemical mapping of highly (U87) vs. poorly (A549/8) angiogenic tumors provided results comparable to culture models. Therefore, FT-IR imaging allows detecting subtle chemical changes in tumors, which might be useful for diagnosis.**

Keywords: FT-IR imaging; Histopathology; Cancer; Metabolism; CAM-assay; Oxidative stress

1. Introduction

Many solid tumors, including glioma and lung carcinoma, pose challenges for disease management and treatment. Beside histopathological evaluation of tumor grade, novel diagnostic tools have been developed, such as gene profiling, aiming to identify prognostic indicators from a variety of molecular parameters associated to the tumor differentiation stages and tissue types.

Analyses of the metabolic pathways involved in tumor development may also provide useful information for disease diagnosis and treatment. Both hypoxia and metabolite deprivation are commonly observed in solid tumors and modulate the transcription of genes involved in several cellular processes, including malignant growth, angiogenesis, and metastasis [1]. As a consequence of hypoxia and of the increased expression of glycolytic enzymes, tumors are prone to consume more glucose than normal tissues, thus participating to its pericellular depletion and to the accumulation of waste products and pH acidification [2]. Solid tumor growth may also induce a local increase in free radicals, leading to the alteration of normal cellular processes through peroxidation of lipids, proteins, and nucleic acids [3]. Tumors also differ widely in their energy requirement, depending on the cell types considered, tumor grade and tissue locations. Thus, a rapid and accurate determination of the spatial metabolic profile of tumors is required for a better diagnosis in order to adopt relevant therapeutic strategies. Biochemical and histological approaches in association to bioluminescence imaging have been developed to address this question [4].

Methods based on Fourier-transform infrared (FT-IR) spectrometry emerged and developed rapidly during the last decade [5]. FT-IR spectra are representative of the whole organic content of biological samples and can therefore be used as molecular signatures of normal and pathological tissues. Reported applications of FT-IR spectrometry in biomedicine consist of molecular structure determination, cancer DNA phenotype recognition and determination of molecular concentration profiles [6,7]. Fast FT-IR spectral imaging systems are now available, allowing the acquisition of tissue functional FT-IR images in only a few minutes.

In this work, we analyzed biochemical parameters using a chemical FT-IR mapping of two human cancer cell types, namely U87 glioma and lung A549/8 adenocarcinoma cells, exposed to hypoxic conditions and/or under glucose deprivation in vitro. U87 and A549/8 malignant cells were also implanted onto the chorio-allantoic membrane (CAM) of the chicken egg [8] to develop solid tumors of highly vs. poorly angiogenic phenotypes, respectively. FT-IR spectral imaging of these tumors allowed the detection of biochemical changes within the different tumor masses at a 6-micrometer spatial resolution.

2. Materials and methods

2.1. Cell culture

Cell culture in serum-free medium was essentially performed as described [9]. Cells were routinely propagated in a humidified 5% CO_2 atmosphere at 37 °C. Hypoxic conditions were obtained at 3% O_2 in a Heraeus incubator BB-6060. For FT-IR experiments, sub-confluent cells in serum-free medium were washed with PBS and incubated for 24 h in serum-free medium containing increasing concentrations of glucose, as indicated in the figure legends. At the end of each experiment, collected cells were centrifuged and pellets ($\sim 10^6$ cells) were quickly re-suspended in 300 μl of ice-cold sterile water and frozen in liquid nitrogen.

*Corresponding author. Address: Univ Bordeaux 2, Bordeaux, F-33000, France. Fax: +33 5 57571005/02.
E-mail address: cyril.petibois@u-bordeaux2.fr (C. Petibois).

Abbreviations: CAM, chorio-allantoic membrane; FT-IR, Fourier-transform infrared

0014-5793/$32.00
doi:10.1016/j.febslet.2007.10.052

2.2. FT-IR spectra acquisition

Culture media or cell lysates (35 μl) were deposited on a 96-well silicon-plate (Bruker, Germany), placed for 1 h into a drying vacuum (2 mm Hg and silica gel), and put into the analysis compartment of a Bruker Tensor-27 spectrometer equipped with a HTS-XT auto sampler. The spectrometer used a Globar (MIR) source (7 V), a KBr beam splitter, and a DTGS/B detector (16–28 °C). Beam diameter at the sample location was 6 mm and sample deposits were 7-μm diameter. Transmittance spectra were obtained using a 2.0 cm^{-1} resolution and 32 co-added scans. Triplicate FT-IR spectra were averaged and made compatible (wavenumber frequencies standardization).

2.3. FT-IR spectra curve fittings

Spectral curve fittings were performed from FT-IR spectra using the Levenberg–Marquardt method as previously described [10] to determine the ν = (CH), $\nu_{as}(CH_3)$, and $\nu_{as}(CH_2)$ absorptions of fatty acyl chains (3100–2800 cm^{-1} spectral interval) and the characteristic ν(C–O) absorptions of glucose (1033 cm^{-1}) and lactic acid (1127 cm^{-1}). Lactic acid and glucose absorptions were compared to the results of enzymatic assays (lactic acid dehydrogenase- and hexokinase-derived assays, respectively; Biosentec, France) to determine molecular IR absorptivities (mM/a.u.).

2.4. In vivo tumor assay and FT-IR imaging

Tumor xenogratfs were obtained using the experimental model of the CAM assay [8]. Five million cells were deposited per egg. Six xenografts were collected for each condition at days 3, 5, and 7 (D3, D5, and D7) after implantation. Photos of tumors were taken under a stereomicroscope (Nikon SMZ800) equipped with a digital camera (Nikon Coolpix 950). Tumor size was determined and xenografts were placed into sterile tubes and frozen into liquid nitrogen. After return to ambient temperature, tumors were laid down flat on cooled glue (polyvinilic alcohol, −20 °C). Longitudinal tissue sections (20 μm in thickness) were performed every ~200 μm using a Cryostat 3050-TM (Leica-Microsystems, France) to analyze tumor mass from the top down to its contact to CAM. Tissue sections were analyzed in the mid-infrared range (4000–620 cm^{-1}) using a Spotlight 300 FT-IR imaging system equipped with a Spectrum-One spectrometer (Perkin–Elmer, Bucks, UK). FT-IR spectra were obtained using 8 co-added scans (4000–700 cm^{-1}) in transmission mode with a spatial resolution of 6.25 μm^2 per pixel and a 4 cm^{-1} spectral resolution.

2.5. FT-IR image data treatment

FT-IR spectra were corrected for CO_2 and H_2O absorptions. Transversal capillary blood vessels were spotted using the visible image. Then, successive 50 μm^2 areas (7 × 7 pixels corresponding to 49 FT-IR spectra) were selected starting from the spotted capillaries up to 450 μm in distance. The 49 FT-IR spectra of every area were averaged and the spectral curve fitting method was applied for determining glucose, lactic acid, and fatty acyl chain IR absorptions. Data are presented as means ± S.D. Correlations between enzymatic assays and FT-IR data were tested using Pearson's coefficient (r) with a P value below 0.05. Mean prediction error (Sx/y) was also determined to assess the robustness of the method.

3. Results and discussion

3.1. Metabolic changes in A549/8 and U87 cells subjected to hypoxia and to glucose deprivation

Glucose and lactic acid concentrations in serum-free culture media were first determined using their most characteristic IR absorptions revealed by the curve fitting of the 1200–900 cm^{-1} spectral interval [10]. Glucose IR absorptivity (Glc_{abs}) at 1033 cm^{-1} was 0.46 mM per spectral area unit (a.u.) and its concentrations ($\dot{C}_{glc}$) in culture media were determined according to the equation: $\dot{C}_{glc}$ (mM) = $Glc_{a.u.} \times Glc_{abs}$. Lactic acid IR absorptivity ($L - A_{abs}$) at 1127 cm^{-1} was 0.187 mM/a.u., its concentration ($\dot{C}_{L-A}$) being determined as follows: $\dot{C}_{L-A}$ (mM) = $L - A_{a.u.} \times L - A_{abs}$.

Glucose concentrations determined in culture media using FT-IR spectrometry were in accordance with those obtained using enzymatic assays ($r = 0.98$; $P = 0.001$). Consistently, the 1033 cm^{-1} (glucose) and 1127 cm^{-1} (lactic acid) IR absorptions were not detected in FT-IR spectra of culture media that did not contained these two metabolites (Fig. 1). Concentrations of glucose and lactic acid in culture media after incubation with metabolically active cells also correlated well with results of enzymatic assays (Supplementary Fig. S1). These results show the compliance of using spectral curve fitting to determine glucose and lactic acid concentrations in culture media using the 1033 and 1127 cm^{-1} IR absorption bands, respectively.

A549/8 and U87 cells were then incubated for 24 h with various amounts of glucose under normoxia or hypoxia. FT-IR spectrometry analyses were performed from both culture med-

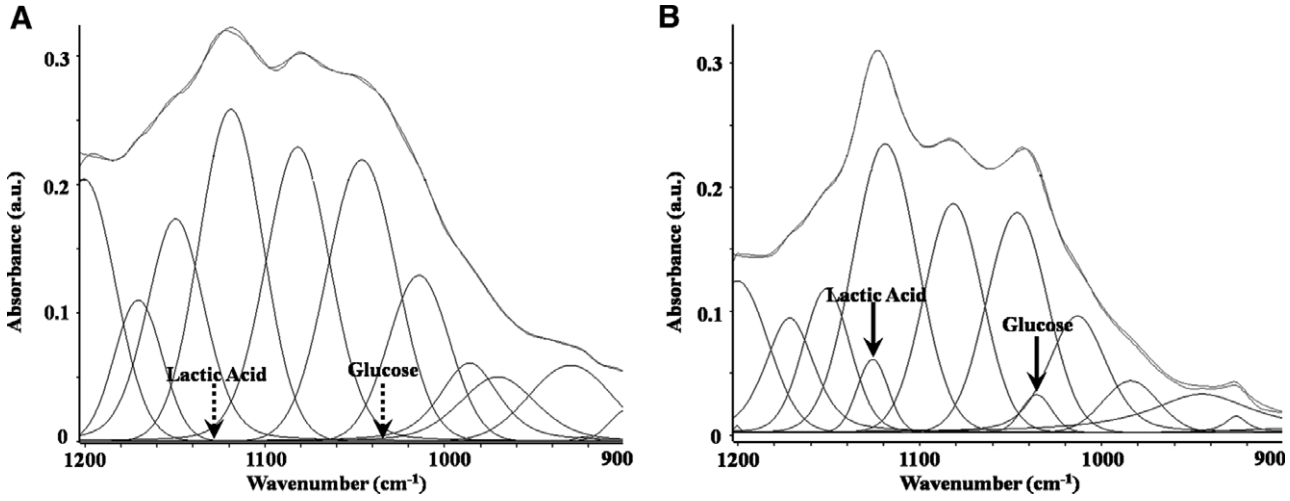

Fig. 1. Detection of glucose and of lactic acid in culture medium and in cell lysates. (A) Curve fitting and deconvolution analyses of the 1200–900 cm^{-1} spectral interval of FT-IR spectra obtained from the serum-free culture medium in the complete absence of glucose and lactic acid. (B) Same experiment as in A except that culture medium contained 1 mM glucose and 1.23 mM lactic acid.

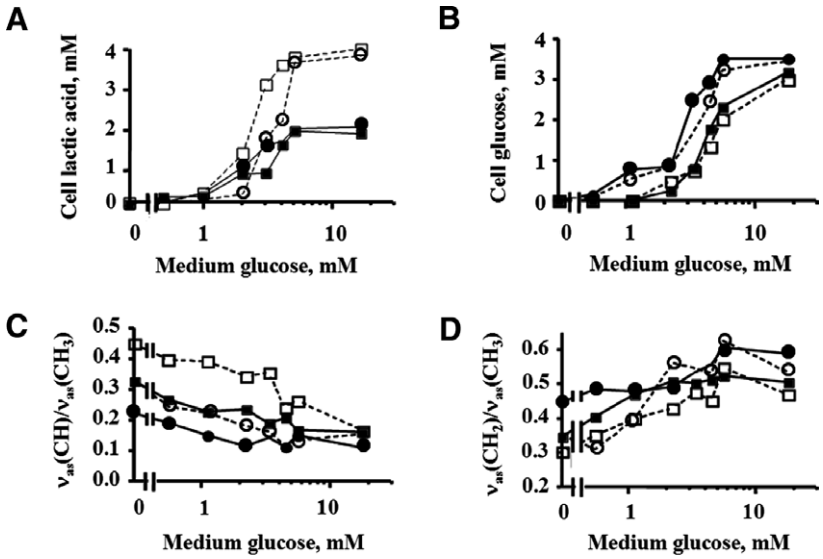

Fig. 2. Post-culture media analyses by FT-IR spectrometry of A549/8 and U87 cell extracts after exposition to normoxia or to hypoxia. Concentrations of lactic acid (A), glucose (B) as well as of fatty acyl moieties absorptions (C, D) changes were determined in A549/8 (●, ○) cells and U87 (■, □) cells that were incubated under normoxia (●, ■) or hypoxia (○, □) for 24 h in serum-free culture medium containing increasing amounts of glucose. IR absorptions of fatty acyl moieties were reported as values of the two ratios $\nu = (CH)/\nu_{as}(CH_3)$ and $\nu = (CH_2)/\nu_{as}(CH_3)$, indicative of the insaturation level of phospholipids and of cellular oxidative stresses, respectively. $\nu = (CH)/\nu_{as}(CH_3)$ ratio values are magnified by 10 for presentation. Each result is the mean of triplicate determination that differed by less of 5%.

ia and cell extracts to compare various aspects of glucose metabolism and of cell oxidation. As shown in Fig. 2A and B, cells subjected to hypoxia contained lower amounts of glucose and higher amounts of lactic acid than cells incubated under normoxia. In addition, glucose consumption was higher in U87 cells than in A549/8 cells. Indeed, a lower glucose concentration was observed in U87 cells than in A549/8 cells in association to a more marked decrease of the metabolite in the culture medium of U87 cells. Consistently, glucose was not detected in A549/8 and U87 cells with initial glucose concentration below 0.5 and 1.11 mM, respectively. Again, enzymatic assays validated the method based on FT-IR spectral curve fitting ($P < 0.05$, not shown).

We next analyzed the variations in $\nu = (CH)$, $\nu_{as}(CH_3)$, and $\nu_{as}(CH_2)$ IR absorptions (Fig. 2C and D) for determining oxidative stress effects on cells. Although possible contributions to these absorptions may stem from metabolic free fatty acids (in very low concentration) and from acetyl groups of proteins, which are very weak in intensity [11], these absorptions are mainly due to fatty acyl moieties of membrane phospholipids of cells [12]. The results obtained from the curve fitting of the 3100–2800 cm^{-1} spectral interval revealed that the $\nu = (CH)/\nu_{as}(CH_3)$ ratio consistently increased in the two cell types exposed to low glucose conditions, a concomitant decrease being observed for the $\nu_{as}(CH_2)/\nu_{as}(CH_3)$ ratio. IR absorptions changes were also more pronounced under hypoxic vs. normoxic conditions. Thus, the results agree well with an expected higher insaturation level of phospholipids under glucose-limiting conditions or under hypoxia [13]. In addition, U87 cells exposed to hypoxia and to low glucose concentrations presented higher insaturation levels of their fatty acyl moieties than A549/8 cells, which may reflect various degrees of peroxidation. The better resistance of A549/8 cells to oxidation may be explained by the natural occurrence of lung epithelial cells in a more oxidizing microenvironment and to their enhanced protection using anti-oxidative defense systems [14].

3.2. Phenotypic changes and FT-IR imaging of tumor tissues

Cancer cells deposited onto the CAM surface form solid tumors that exhibit characteristic features of malignant progression [8]. Phenotypic changes of A549/8 cell- and U87 cell-derived tumors were analyzed 3, 5, and 7 days following implantation. U87 cell-derived xenografts grew rapidly and formed a compact tumor mass at day 3. Tumors then expanded as determined by diameter measurement at days 5 (2.2-fold, $P < 0.01$) and 7 (3.5-fold, $P < 0.01$) (Fig. 3A). A549/8 cell-derived tumor diameters also increased as a function of time, although at a lesser rate (1.4-fold, $P < 0.05$ at D5; 2.7-fold, $P < 0.01$ at D7).

The two types of tumors also exhibited different angiogenic patterns. Poorly vascularized A549/8 A549/8 cell-derived tumors usually presented a general whitish aspect whereas highly angiogenic U87 cell-derived tumors are pinkish/red in relation to the intensity of angiogenesis. A few blood vessels were observed at day 3 in all (6/6) A549/8 cell-derived tumors, which is consistent with the fact that pericytes were not detected in the tumor masses (Fig. 3D and G). The number of blood vessels then progressively increased at day 5 in two out of the six tumors analyzed (Fig. 3E and H). Finally, all tumors presented at day 7 a structured vascular network into the whole tumor mass, with capillaries 100–300 μm distant from each other (Fig. 3F and I). An increased spreading of pericytes was also detected in tumor tissues at days 5 and 7 (Fig. 3H and I). The neovascularization process was also analyzed in U87 cell-derived xenografts. At day 3, none of the six tumors presented any detectable vascular network whereas an extensive vascular network developed in all tumors at days 5 and 7 (not shown, see also Ref. [8]).

Serial visible images of the tumor tissue section were used to confirm the tumor morphology and angiogenic status before FT-IR spectral imaging was performed (Fig. 3B). Three to seven tissue sections (every ~200 μm) covering the thickness of the tumors were used for FT-IR images acquisition. Spatial dis-

tribution of glucose, lactic acid, and fatty acyl chain IR absorptions was measured in inter-capillary spaces by selecting successive 50 μm^2-areas units (Fig. 3C). Glucose and lactic acid absorptions as well as the $\nu_{as}(CH_2)/\nu_{as}(CH_3)$ and $\nu = (CH)/\nu_{as}(CH_3)$ ratios were determined in each unit and gradient analyses for A549/8 cell-derived tumors are presented in Fig. 4. As shown, glucose absorption was expressed as a U-shaped curve, with the higher values being detected at the edge of capillaries (Cap.1 and Cap.2) and lower values being obtained at a 150–200 μm distance from the capillaries, above the critical diffusion distance for oxygen and nutrients [2]. Consistently, lactic acid absorption change was expressed as an inverted curve regarding that of glucose, which relates to the decreased capacity of tissues to eliminate metabolic wastes as the distance to capillaries increases. Similar results were obtained with the two cell types, even though glucose consumption and lactic acid release were higher in U87-derived tumors (Supplementary Fig. S2) than in A549/8-derived tumors. These results are consistent with those obtained in cell culture.

We next addressed the question of the possible metabolic variation in tumor microenvironments as a function of their growth stage. Spectral curve fitting for the 1200–900 cm^{-1} and 3100–2800 cm^{-1} spectral intervals were performed on 50 μm^2 tissue areas found at a 200-μm distance from any blood capillaries. Analyses performed with A549/8 cell-derived tumors at the whole section scale following 3 days of tumor growth showed that no significant spatial variation was observed in glucose and lactic acid absorptions, or in the $\nu = (CH)/\nu_{as}(CH_3)$ and $\nu_{as}(CH_2)/\nu_{as}(CH_3)$ ratios (Fig. 5A–D; see also results on U87 cell-derived tumors, Supplementary Fig. S3). Besides, a spatial heterogeneity in molecular content was observed at days 5 and 7 in relation to the vascularization status. FT-IR measurements were therefore determined both at the immediate vicinity of blood capillaries and at a 200-μm distance from blood capillaries. Glucose and lactic acid absorption values at the edge of capillaries were found similar at days 5 and 7 and did not differ significantly from the values obtained at day 3 ($N = 35$) (Fig. 5A and B). In contrast, measurements performed at ~200 μm from blood capillaries at days 5 and 7 showed that glucose significantly decreased at a distal position from blood supply ($N = 24$) whereas that of lactic acid correlatively increased.

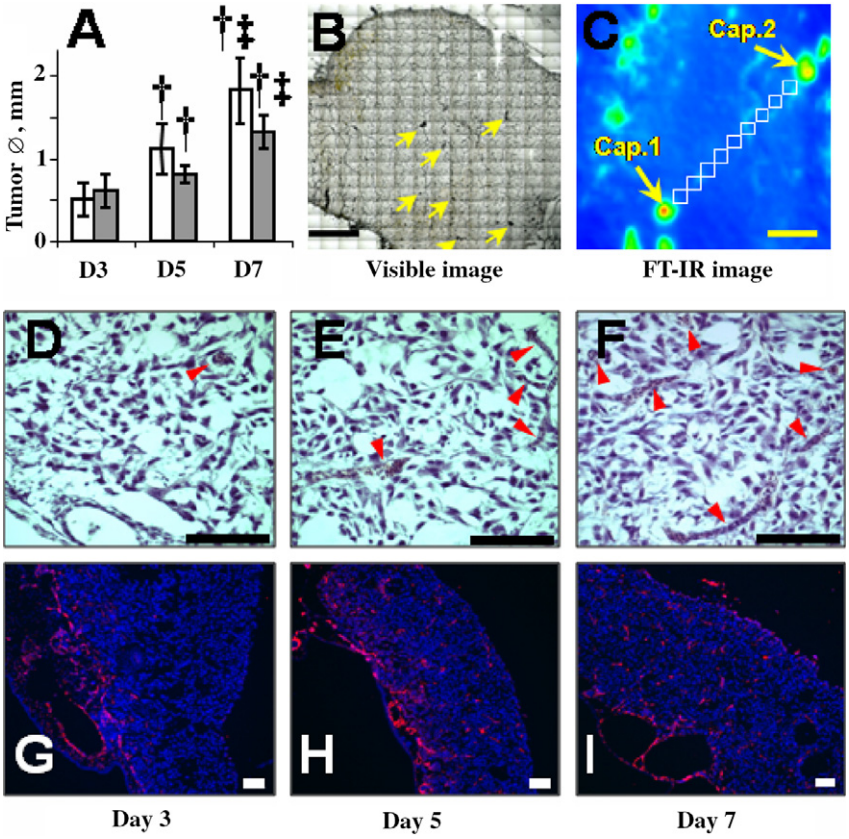

Fig. 3. Changes in tumor growth and angiogenesis in the CAM assays. (A) Tumor growth measurement. U87 cells (white bars) and A549/8 cells (grey bars) were implanted onto the CAM and tumors were grown for 3, 5, and 7 days (D3, D5, and D7, respectively). (B) Example of visible image (black bar = 500 μm; 10× magnification using a Nikon SMZ stereomicroscope) obtained from a cryosection of A549/8 cell-derived tumor tissue section (20-μm thickness) and (C) FT-IR image obtained with the same cell deposit at day 7 with a 6.25 μm resolution per pixel (yellow bar = 200 μm; full spectral absorbance). Arrows in (B) and (C) indicate the presence of blood capillaries. Successive tissue areas (50 × 50 μm = 9 × 9 spectra) were selected between two blood capillaries reported as Cap.1 and Cap.2 and spectral curve fitting was applied on averaged spectra for determining the spatial distribution of glucose and lactic acid as well as IR absorption changes for fatty acyl moieties. (D–F) Histological examinations performed on A549/8 cell-derived tumors 3, 5, and 7 days after implantation, respectively. Tumors were cut into 10 μm cryosections and stained with H&E for histological analyses and observation of the vascularization. Nucleated chick erythrocytes, blood vessels lining and red labeling revealed tumor capillaries which are indicated by red arrowheads. (G–I) Immunofluorescence labeling of pericytes using mouse antibodies directed against desmin at days 3, 5, and 7 after implantation, respectively.

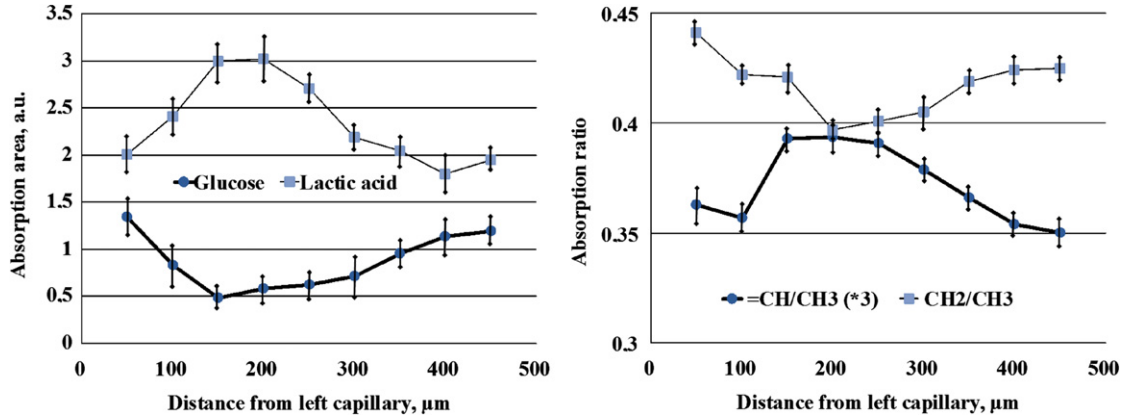

Fig. 4. Chemical mapping of A549/8 cell-derived tumor development 7 days after implantation. Tumors were removed from the CAM and snap frozen in liquid nitrogen. Twenty-µm serial cryosections were processed for FT-IR spectrometry. Analyses were performed in different tumor areas. Biodistribution of glucose and lactic acid (left) as well as the changes in the $\nu_{as}(CH_2)/\nu_{as}(CH_3)$ and $\nu = (CH)/\nu_{as}(CH_3)$ ratios (right) were determined according to the distance from capillaries.

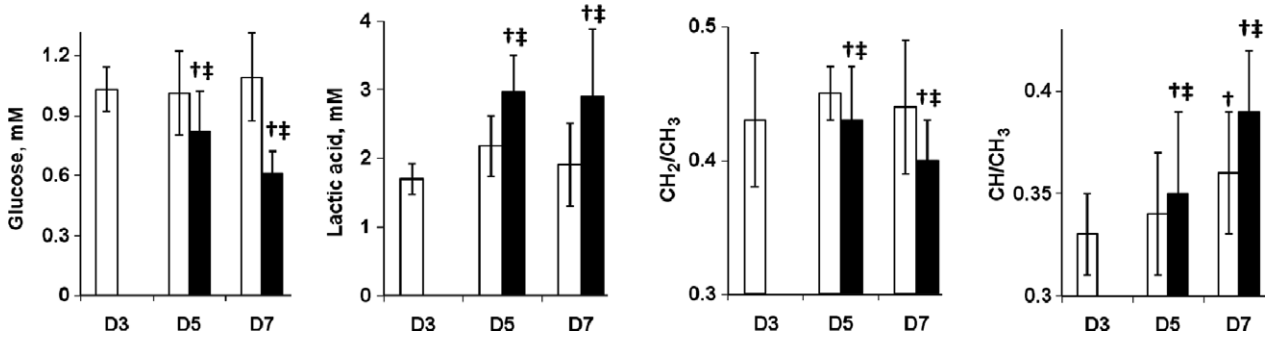

Fig. 5. Chemical mapping of A549/8 cell-derived tumors analyzed at days 3 ($n = 6$), 5 ($n = 16$), and 7 ($n = 31$) after implantation. Spectral curve fitting for the 1200–900 cm^{-1} and 3100–2800 cm^{-1} spectral intervals were performed on the 50×50 µm tissue areas found at the vicinity (white bars) and at a 200-µm distance (black bars) from any blood capillaries for determining the glucose, lactic acid, and fatty acyl moieties absorption in tumors. †: significantly different from value obtained with the preceding measurement at D-2; ‡: significantly different from measurements at the vicinity of blood capillaries. $P < 0.05$.

Variations in fatty acyl moieties absorptions were also observed in different sub-regions of the tumors (Fig. 5C and D). Higher $\nu = (CH)/\nu_{as}(CH_3)$ ratios were obtained at distances greater than 200 µm from capillaries at day 5 ($P < 0.01$) and day 7 ($P < 0.01$) associated to a concomitant decrease of the $\nu_{as}(CH_2)/\nu_{as}(CH_3)$ ratio ($P < 0.01$ at days 5 and 7). This suggests that the oxidative environment differed in discrete regions of the tumors in relation to glucose degradation and lactic acid production. Similar results were obtained using U87 cell-derived tumors (Supplementary Fig. S3).

Taken together, these results indicate that FT-IR imaging is a valuable tool for detecting spatial metabolic changes within tumors. This approach may therefore be useful in deciphering in situ biochemical aspects of tumor development, including altered metabolism regulation and oxidative stress effects.

3.3. FT-IR imaging for a molecular histopathology

Various non-invasive technologies allow clinical examinations of tumor tissues. However, the use of contrast reagents is often required due to a poor sensitivity (MRI) and/or a poor resolution (PET). Still, their applications remain limited to medium- and large-size specimens. Therefore, there is a need for an imaging technique able to provide real time information on the metabolic and structural status of smaller tissues. In the context of surgical resection of tumors, FT-IR imaging appears as a promising technique to rapidly generate multiparametric information from biochemical events underlining a pathological status [6,15], as exemplified in this study by the tissue distribution of glucose and lactic acid in tumors. Critical information on structural modifications of macromolecules may also be obtained, as shown for the measurement of fatty acyl chains peroxidation level. Thus, FT-IR imaging may be developed into a valuable method for the rapid detection of diagnosis and prognosis markers of malignant diseases.

Acknowledgement: The authors are indebted to the Regional Council of Aquitaine, the National Center for Scientific Research (CNRS), the ARC (Grant 3694), the University Bordeaux 1 (BQR 2005) and the "Ligue régionale contre le cancer" for financial support.

Appendix A. Supplementary data

Supplementary data associated with this article can be found, in the online version, at doi:10.1016/j.febslet.2007.10.052.

References

[1] Pouysségur, J., Dayan, F. and Mazure, N.M. (2006) Hypoxia signalling in cancer and approaches to enforce tumour regression. Nature 441, 437–443.

[2] Gatenby, R.A. and Gillies, R.J. (2004) Why do cancers have high aerobic glycolysis? Nat. Rev. Cancer 4, 891–899.

[3] Trachootham, D. et al. (2006) Selective killing of oncogenically transformed cells through a ROS mediated mechanism by b-phenylethyl isothiocyanate. Cancer Cell 10, 241–252.

[4] Schroeder, T., Yuan, H., Viglianti, B.L., Peltz, C., Asopa, S., Vujaskovic, Z. and Dewhirst, M.W. (2005) Spatial heterogeneity and oxygen dependence of glucose consumption in R3230Ac and fibrosarcomas of the Fischer 344 rat. Cancer Res. 65, 5163–5171.

[5] Ellis, D.I. and Goodacre, R. (2006) Metabolic fingerprinting in disease diagnosis: biomedical applications of infrared and Raman spectroscopy. Analyst 131, 875–885.

[6] Petibois, C. and Déléris, G. (2006) Chemical mapping of tumor progression by FT-IR imaging: towards molecular histopathology. Trends Biotechnol. 24, 455–462.

[7] Fernandez, D.C., Bhargava, R., Hewitt, S.M. and Levin, I.W. (2005) Infrared spectroscopic imaging for histopathologic recognition. Nat. Biotechnol. 23, 469–474.

[8] Hagedorn, M., Javerzat, S., Gilges, D., Meyre, A., de Lafarge, B., Eichmann, A. and Bikfalvi, A. (2005) Accessing key steps of human tumor progression in vivo by using an avian embryo model. Proc. Natl. Acad. Sci. USA 102, 1643–1648.

[9] Drogat, B., Bouchecareilh, M., Petibois, C., Déléris, G., Chevet, E., Bikfalvi, A. and Moenner, M. (2007) Acute L-glutamine deprivation compromises VEGF-A up-regulation in A549/8 human carcinoma cells. J. Cell Physiol. 212, 463–472.

[10] Petibois, C., Gionnet, K., Goncalves, M., Perromat, A., Moenner, M. and Déléris, G. (2006) Analytical performances of FT-IR spectrometry and imaging for concentration measurements within biological fluids, cells, and tissues. Analyst 131, 640–647.

[11] Petibois, C. and Déléris, G. (2004) Oxidative stress effects on erythrocytes determined by FT-IR spectrometry. Analyst 129, 912–916.

[12] Petibois, C. and Déléris, G. (2005) Evidence that erythrocytes are highly susceptible to exercise oxidative stress: a FT-IR spectrometry study at the molecular level. Cell Biol. Int. 29, 709–716.

[13] Guppy, M. (2002) The hypoxic core: a possible answer to the cancer paradox. Biochem. Biophys. Res. Commun. 299, 676–680.

[14] Ahmad, A., Ahmad, S., Schneider, B.K., Allen, C.B., Chang, L.Y. and White, C.W. (2002) Elevated expression of hexokinase II protects human lung epithelial-like A549 cells against oxidative injury. Am. J. Physiol. Lung Cell Mol. Physiol. 283, L573–L584.

[15] Levin, I.W. and Bhargava, R. (2005) Fourier transform infrared vibrational spectroscopic imaging: integrating microscopy and molecular recognition. Annu. Rev. Phys. Chem. 56, 429–474.